Dissociation Characteristics of $[M + X]^+$ Ions (X = H, Li, Na, K) from Linear and Cyclic Polyglycols

Thomas L. Selby and Chrys Wesdemiotis
Department of Chemistry, The University of Akron, Akron, Ohio, USA

Robert P. Lattimer
The BFGoodrich Research and Development Center, Brecksville, Ohio, USA

The unimolecular reactions of protonated and metalated polyglycols with kiloelectronvolt translational energies have been studied by collisionally activated dissociation and neutralization–reionization mass spectrometry. The former method provides information on the ionic dissociation products, whereas the latter allows for the identification of the complementary neutral losses. Protonated linear polyglycols mainly undergo charge-initiated decompositions that lead to eliminations of smaller oligomers. On the other hand, protonated crown ethers ("cyclic" polyglycols) favor charge-induced reactions that proceed by cleavages of two ethylene oxide units in the form of 1,4-dioxane. Replacement of one O by NH in the crown ether dramatically changes its unimolecular chemistry; now, charge-remote 1,4-eliminations from ring-opened isomers are preferred. Charge-remote reactions are also the major decomposition channels of all metalated precursors studied. The linear polyglycols decompose primarily by 1,4-H_2 eliminations and to a lesser extent by homolytic cleavages near chain ends. The reverse is true for metalated crown ethers, which preferentially produce distonic radical cations by the loss of saturated radicals; these reactions are proposed to involve prior rearrangement to open-chain isomers. The nature of the metal ion (Li^+, Na^+, or K^+) does not greatly affect the unimolecular chemistry of the cationized polyglycol. In general, metalated precursors form many abundant fragment ions over the entire mass range; hence, collisional activation of such ions at high kinetic energy should be particularly useful for structure elucidations. *(J Am Soc Mass Spectrom 1994, 5, 1081–1092)*

Polyglycols represent a commercially important class of low molecular weight polar polymers. Their analysis by tandem mass spectrometry [1] has experienced a steady growth after desorption ionization methods [2] enabled the volatilization and ionization of these thermally labile materials. In the most common approach, the polyglycol sample (M) is converted to gaseous quasimolecular ions $[M + X]^+$ by fast-atom bombardment (FAB) [3, 4]. In the positive FAB mode, a proton or alkali metal cation (X^+) is attached to M to form an $[M + X]^+$ adduct, which is later mass-selected and subjected to collisionally activated dissociation (CAD), leading to structurally diagnostic fragments [1].

Thus far, the vast majority of polyglycol FAB tandem mass spectrometry studies have involved low energy (≈ 50 eV) CAD [5–9]. Under these conditions, X in $[M + X]^+$ determines what types of dissociations predominate. Protonated ions (X = H) almost exclusively undergo charge-initiated decompositions [5, 8]. On the other hand, lithiated species (X = Li) yield fragments by both charge-site and charge-remote reactions [10], whereas little fragmentation is observed from Na^+ or K^+ attachment ions [5, 6, 9]. The charge-remote decompositions of $[M + Li]^+$ were found to have superior analytical value [6, 9]. Charge-remote reactions usually require relatively large critical energies and should be more favored in high energy CAD (kiloelectronvolt domain) [10]. For this reason, the present study examines the unimolecular chemistry of polyglycol $[M + X]^+$ cations under high energy collision conditions. Investigated were H^+, Li^+, Na^+, and K^+ attachment ions from the linear and cyclic molecules summarized in Table 1.

With kiloelectronvolt tandem mass spectrometry experiments, it also is possible to elucidate the neutral fragments that arise during the CAD process. This is achieved by using the neutralization–reionization mass spectrometry (NRMS) methodology [11–13]. In a NRMS type experiment, the ionic CAD products are removed from the beam path by electrostatic deflection, and the remaining neutral losses are post-ionized and detected in neutral fragment-reionization (N_fR)

Address reprint requests to Chrys Wesdemiotis, Department of Chemistry, The University of Akron, Akron, OH 44325-3601.

1044-0305/94/$7.00

Received May 31, 1994
Revised July 15, 1994
Accepted July 25, 1994

Table 1. Polyglycols studied

Structure	Nomenclature		Mass u
$HO-(CH_2-CH_2-O)_n-H$	Poly(ethylene glycol) (PEG)	1[a]	458
$CH_3O-(CH_2-CH_2-O)_n-H$	PEG monomethyl ether (PEGME)	2[a]	472
$CH_3O-(CH_2-CH_2-O)_n-CH_3$	PEG dimethyl ether (PEGDME)	3[a]	486
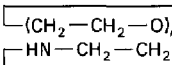	15-Crown-5[b] ($n = 5$)	4	220
	18-Crown-6[b] ($n = 6$)	5	264
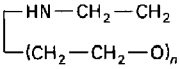	1-Aza-18-crown-6 ($n = 5$)	6	263

[a] The decamers ($n = 10$) of these polymers were investigated.
[b] The first and last numbers refer to the total number of atoms and the number of heteroatoms, respectively.

mass spectra [14]. The N_fR spectrum of an $[M + X]^+$ precursor ion contains all neutrals liberated from $[M + X]^+$. Each neutral loss generates, on reionization, its own collision-induced dissociative ionization (CIDI) mass spectrum [15]; hence, the ultimately observed N_fR spectrum is comprised of the superimposed CIDI spectra of the individual neutral fragments. Despite this convolution, neutral fragment-reionization can help identify what types of neutrals are formed upon CAD [15–19]. As will be shown here, such information, combined with that stored in the conventional CAD spectra, provides invaluable insight on the fragmentation mechanisms of the $[M + X]^+$ precursor cations.

Experimental

The experiments described were performed with a VG AutoSpec (VG Fisons Ltd., Manchester, UK) E_1BE_2 tandem mass spectrometer [20], in which E_1B served as mass spectrometer 1 (MS-1) and E_2 as mass spectrometer 2 (MS-2). This instrument is equipped with three collision cells (Cls). One (Cls-1) is situated in the field-free region following the ion source (FFR-1); two further collision cells (Cls-2 and Cls-3), with an intermediate deflector, are located in the region between the magnet and the second electric sector (FFR-3).

The materials were ionized by FAB, using a Cs^+ ion gun (operated at ~ 20 keV) as the source of primary particles. A few micromoles of sample were applied onto the FAB probe tip without matrix. Formation of $[M + X]^+$ was promoted by adding trifluoroacetic acid for X = H or the appropriate alkali iodide for X = Li, Na, and K. $[M + X]^+$ was accelerated to 8 keV, mass-selected by MS-1, and subjected to CAD with He in Cls-2. The ionic fragments formed were recorded in the respective CAD spectrum by scanning MS-2. For the detection of the complementary neutral losses, all ions exiting Cls-2 were electrostatically deflected, and the remaining beam of neutral fragments was cationized by collision with O_2 in Cls-3. The newly formed ions were mass-analyzed through MS-2 and collected in the neutral fragment-reionization (N_fR He/O_2) spectrum of $[M + X]^+$. The CIDI spectrum of triethylene glycol (TEG) was obtained similarly by dissociating the corresponding proton-bound dimer, M_2H^+; on CAD, this dimer ion dissociates mainly (> 80%) via $M_2H^+ \rightarrow MH^+ + M$, producing a beam of relatively pure TEG molecules. (Because one principal neutral fragment is eliminated, the N_fR spectrum of M_2H^+ essentially matches the CIDI spectrum of M [14, 17].) CAD spectra also were measured in FFR-1 by using Cls-1 and linked scanning [1]. These spectra (not shown) are qualitatively similar to those obtained in FFR-3. The better fragment ion resolution in the linked scans [1] facilitated (and/or confirmed) product ion assignments in the spectra acquired by E_2 scans in FFR-3.

The pressures of the collision gases were adjusted to effect ~ 30% beam attenuation in each collision cell. Under these conditions, the reionization efficiency of the neutral losses from the various precursor ions studied ranges between 0.02–0.3%; that of pure TEG is 0.04%. These efficiencies were calculated by dividing the total ion current in the N_fR spectrum by the flux of neutral fragments. The latter is assumed to be equal to the flux of the complementary ionic fragments detected in the respective CAD spectrum [17]. Overall, the total ions after N_fR are 4–5 orders of magnitude weaker than the precursor ion intensity.

A reference spectrum of 1,4-dioxane was acquired by neutralizing its molecular cation, generated by 70-eV electron ionization (EI), with Xe and reionizing the neutral beam with O_2. This experiment was performed at 2.7 keV, that is, at the kinetic energy with which dioxane is eliminated from protonated 18-crown-6 (vide infra). The reionization efficiency of dioxane (total ions in neutralization–reionization spectrum normalized to the neutral beam intensity) is ~ 0.3% at 2.7 keV and ~ 2% at 8 keV. The latter value is similar to the reported O_2 reionization efficiency of 10-keV ethylene oxide [21].

The spectra shown are multiscan summations and their relative abundances are reproducible within ±20%; the error limit for absolute intensities (i.e., for N_fR and reionization yields) is better than ±50%. The N_fR figures display only the mass-to-charge ratio range that contains discernible peaks. The compounds stud-

ied were purchased from Aldrich Chemical Co. (Milwaukee, WI) and introduced into the mass spectrometer without alteration.

Results and Discussion

$[M + H]^+$ Precursor Ions

$[M + H]^+$ of Poly(ethylene glycol) Decamer and Its Mono- and Dimethyl Ethers (1–3). The prominent fragment ions in the CAD spectrum of $[1 + H]^+$ (Figure 1a) belong to the series **A** (Scheme I), which is nominally generated by inductive (*i*), that is, charge-site catalyzed, cleavages. The incipient ionic products of these decompositions would be primary carbonium cations, as depicted in Scheme I; such ions are prone to isomerization [22] and may rearrange to more stable structures [23] during or after their formation.

From the dimethyl derivative $[3 + H]^+$, a homologous ion series (**A'**) is obtained (Figure 1c) and appears 14 u above the **A** series. Also the **A'** type fragments are consistent with a charge-site initiated dissociation mechanism (Scheme II). Expectedly, CAD of the monomethylated cation $[2 + H]^+$ leads to a mixture of **A** and **A'** fragments (Figure 1b), because the charge can remain at either side of the now nonsymmetrical protonated ether linkage.

The neutral fragments that accompany these charge-site decay reactions can be elucidated from the corresponding N_fR spectra (Figure 2). Before proceeding with the interpretation of these data, it is important to recognize that collisional ionization imparts high internal energies, thus causing extensive fragmentation [24, 25]. This is illustrated for triethylene glycol (TEG) in Figure 3. A relatively pure beam of neutral TEG can be produced by dissociation of the proton-bound dimer, namely, $(TEG)_2H^+ \rightarrow [TEG + H]^+ + TEG$. Collisional ionization of the so liberated TEG yields the collision-induced dissociative ionization (CIDI) spectrum of Figure 3, which shows similar fragments to those observed in the EI spectrum of TEG [26]. Note, however, that the abundances of unsaturated fragments (e.g., of m/z 87, 73, and 43) are markedly larger in the CIDI as compared to the EI spectrum. Because formation of unsaturated ions requires higher activation energies than formation of more saturated analogs [22, 23], this result points out that CIDI can deposit, on average, more excitation than electron impact [25]. As a consequence, N_fR spectra are often dominated by low mass products and may not contain the intact molecular ions of the neutral losses [17–19].

The N_fR spectrum of $[1 + H]^+$ (Figure 2a) includes all ions present in the reference CIDI spectrum of triethylene glycol. Furthermore, the products at m/z 45, 89, and 133 in Figure 2a belong to the **A** series, which is characteristic for polyglycols (vide supra). Hence, the N_fR spectrum of $[1 + H]^+$ supports Scheme

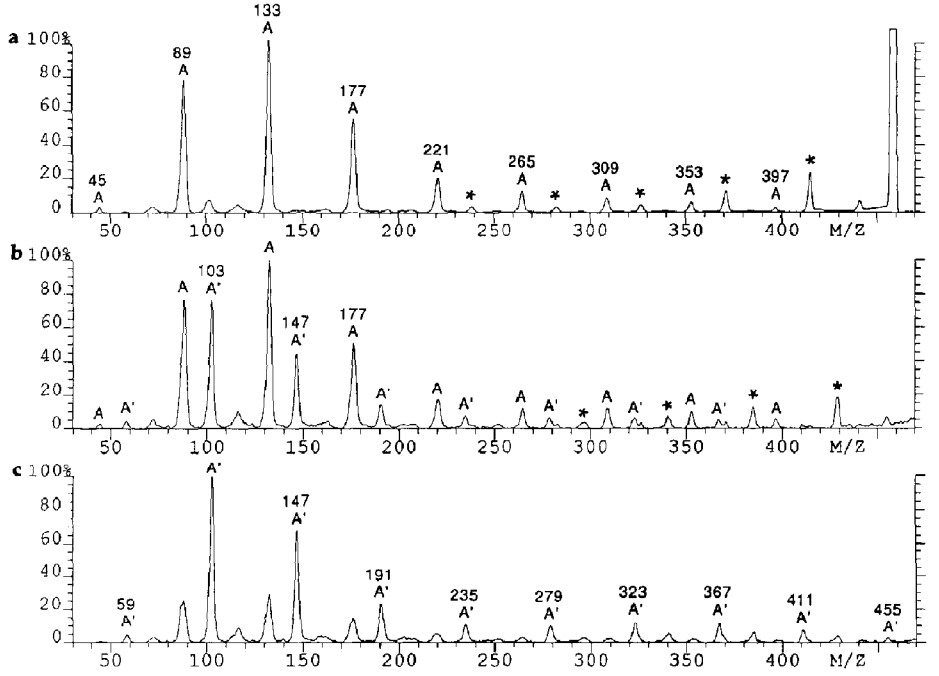

Figure 1. CAD mass spectra of protonated linear polyglycols: (a) $[1 + H]^+$ (m/z 459), (b) $[2 + H]^+$ (m/z 473), and (c) $[3 + H]^+$ (m/z 487). The **A** and **A'** ions marked appear at m/z 45 + 44x and 59 +44x, respectively. The asterisks indicate fragments from $(C_2H_4O)_n$ losses.

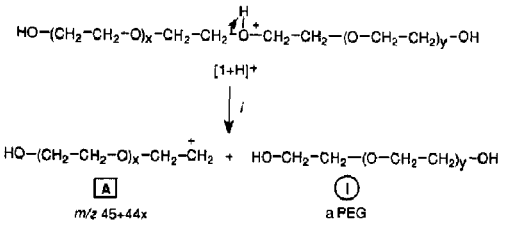

Scheme I

I by confirming that the major neutral losses from protonated PEG are mixtures of smaller PEGs (designated as class I neutrals). $[1 + H]^+$ contains ten ethylene glycol units and can therefore lose PEG oligomers that are larger than TEG; this explains the higher proportion of heavier ions in Figure 2a vis à vis Figure 3.

The N_fR spectrum of $[3 + H]^+$ (Figure 2c) displays members of both series **A** and **A'**. This agrees well with the charge-site decompositions postulated in Scheme II, which release PEGMEs (class II neutrals). Collisional ionization of **II** can yield **A** or **A'** type fragments, depending on whether the charged product carries the hydroxyl or methoxy terminus of **II**, respectively. From precursor ion $[2 + H]^+$, the major neutral losses should be a mixture of **I** and **II** type neutrals. Indeed, this is corroborated by the corresponding N_fR spectrum (Figure 2b), which is dominated by the **A**

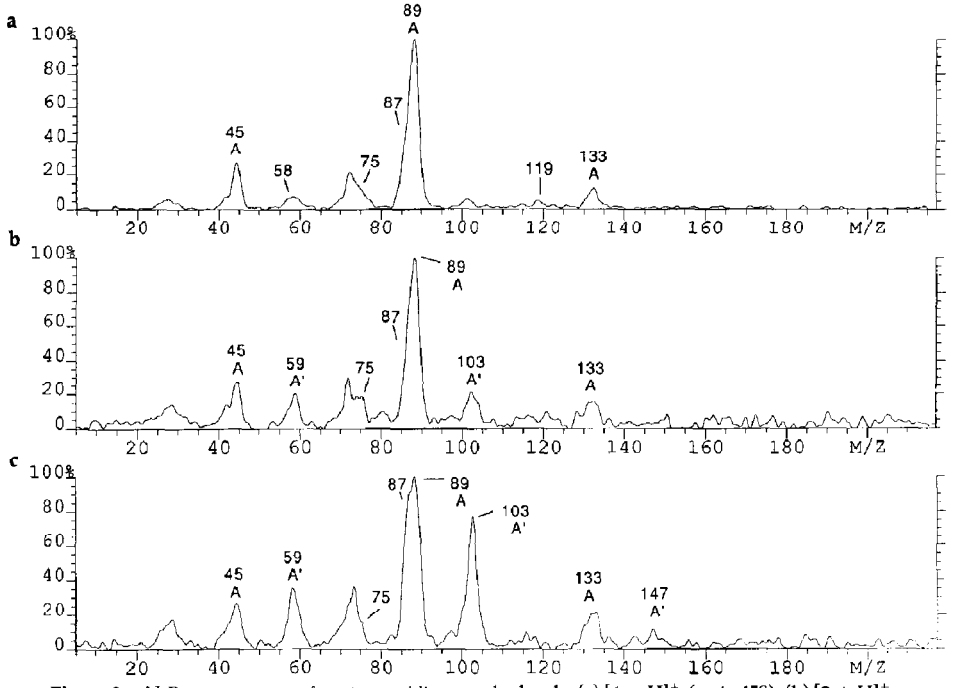

Figure 2. N_fR mass spectra of protonated linear polyglycols: **(a)** $[1 + H]^+$ (m/z 459), **(b)** $[2 + H]^+$ (m/z 473), and **(c)** $[3 + H]^+$ (m/z 487). The **A** and **A'** ions marked appear at m/z 45 + 44x and 59 + 44x, respectively.

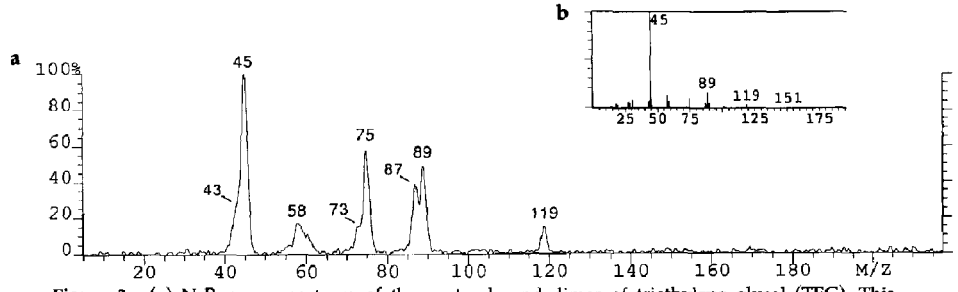

Figure 3. **(a)** N_fR mass spectrum of the proton-bound dimer of triethylene glycol (TEG). This spectrum represents a reference CIDI mass spectrum of TEG. **(b)** Electron ionization spectrum of TEG [26].

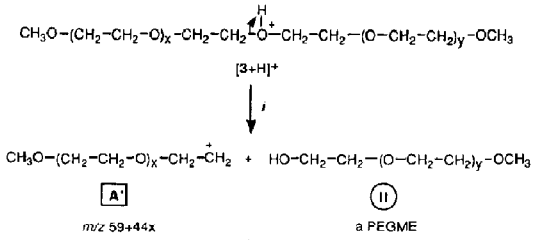

Scheme II

series (feasible from I and II) but also contains some **A'** type cations (feasible from II only).

The largest possible neutral losses of type I and **II** are the PEG nonamer (414 u) and its monomethyl ether (428 u), respectively. However the largest ions observed in the N_fR spectra of Figure 2 are at m/z 133 and 147. This is due to the aforementioned extensive dissociation that takes place during collisional reionization. Nevertheless, the products present in the N_fR spectra provide sufficient information to characterize the nature of neutral fragments cleaved and clearly exclude the possibility that a substantial fraction of series **A** and **A'** in the CAD spectra arises by consecutive eliminations of C_2H_4O monomer units (44 u).

A group of minor fragments in the CAD spectra of $[1 + H]^+$ and $[2 + H]^+$ originates by nominal losses of $(C_2H_4O)_n$ [labeled by asterisk (*) in Figure 1]. Most intense are the ruptures of C_2H_4O ($n = 1$) and $C_4H_8O_2$ ($n = 2$). This series is negligible for $[3 + H]^+$. The overall yield of these reactions is too small for a significant contribution to the N_fR spectra; they probably proceed by a pathway analogous to the $(C_2H_4O)_n$ eliminations from crown ether H^+ attachment ions (see next section).

The high energy CAD spectra of protonated **1**–**3** are most similar to the reported low energy CAD spectra acquired at the lowest possible pressure [8], that is, under single collision conditions [1]. In both cases, all members of the **A** or **A'** series are observed, and the relative intensities of the smaller fragments are larger (see Figure 1). In kiloelectronvolt CAD, the relative abundances are not greatly affected in the ~ 80–50% transmittance range. In contrast, higher collision gas pressures in the electronvolt domain experiments lead to multiple collisions that deplete the larger fragments by dissociating them further [8]; this causes many members of the **A** and **A'** series to disappear and, thus, important structure information is lost.

*$[M + H]^+$ of 15-Crown-5 and 18-Crown-6 (**4**–**5**).* CAD of $[4 + H]^+$ and $[5 + H]^+$ mainly produces **A** type cations (Figure 4), formed by elimination of $(C_2H_4O)_n$. It is noteworthy that the ions emerging by nominal loss of an even number of C_2H_4O units are particularly intense. This characteristic also has been observed in the low energy CAD spectra of protonated **4** and **5** [8]. A plausible reason is that an even number of C_2H_4O can be cleaved in the form of 1,4-dioxane, as illustrated in Scheme III. One dioxane molecule is thermodynamically much more stable ($\Delta H^\circ_f = -316$ kJ/mol [23]) than two separate ethylene oxide molecules ($\Sigma\Delta H^\circ_f = -105$ kJ/mol [23]), which justifies the incentive for losing the former.

The reported EI and CI mass spectra of **4** and **5** also contain the **A** series [27]. The two most abundant ions appear at m/z 45 and 89 and have been proposed to arise by elimination of dioxane from larger fragments. The preference for this dissociation channel has been attributed to the secondary structure (i.e., ring conformation) of crown ether ions [27, 28], which may favor the cleavage of a dioxane molecule by bringing specific ring atoms into proximity (viz. Scheme III).

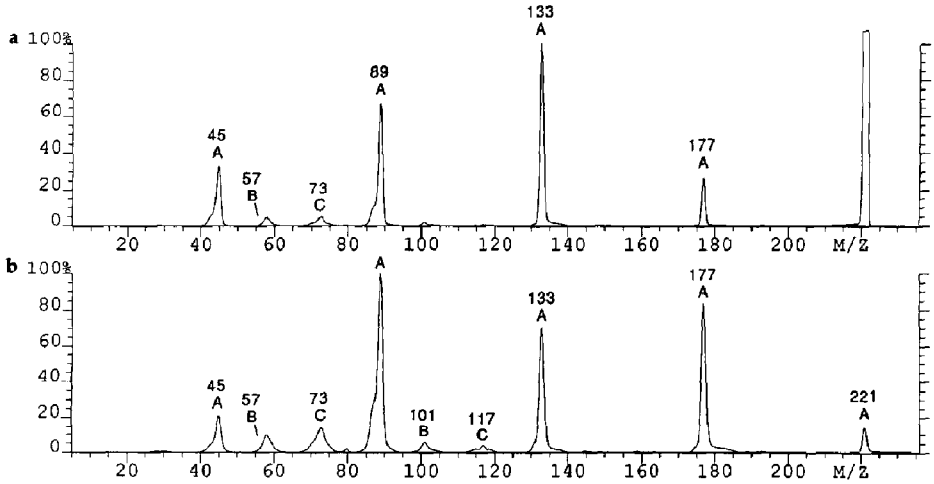

Figure 4. CAD mass spectra of protonated crown ethers: **(a)** $[4 + H]^+$ (m/z 221) and **(b)** $[5 + H]^+$ (m/z 265). The **A**, **B**, and **C** ions marked appear at m/z $45 + 44x$, $57 + 44x$, and $73 + 44x$, respectively.

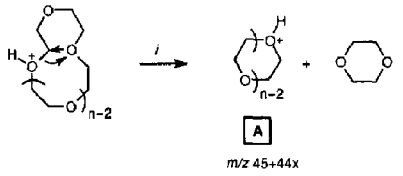

Scheme III

Supporting evidence for the presence of dioxane ($C_4H_8O_2$) in the neutral loss mixture from $[5 + H]^+$ is found in the corresponding N_fR spectrum (Figure 5), which includes $C_4H_8O_2^{+\cdot}$ (m/z 88) and all fragments indicative of dioxane, for example, m/z 43 and 58 based on the EI [26] and neutralization–reionization (Xe/O_2) spectra of this molecule. Ions above m/z 88 are practically absent, which suggests that neutrals larger than dioxane are not eliminated during the formation of **A** fragment ions. In that case, the nominal losses of an odd number of C_2H_4O moieties must involve cleavages of dioxane molecule(s) plus at least one ethylene oxide molecule (monomer). Because of its low kinetic energy (1.3 keV), the monomer is susceptible to scattering and transmission losses [1, 17–19, 29] more severely than dioxane and should contribute less to the N_fR spectrum of $[5 + H]^+$ in spite of comparable reionization cross sections (see Experimental). The C_2H_4O monomer may be a partial source of the $C_2H_4O^{+\cdot}$ cation (m/z 44) in Figure 5, because m/z 44 is the base peak in the reported EI [26] and neutralization–reionization (Hg/O_2) [21] spectra of ethylene oxide.

The fragments labeled with **B** and **C** in Figure 4 formally emerge by charge-remote reactions, similar to those encountered with the NH-substituted crown ether **6** (see next section). The corresponding neutral losses are presumably the origin of the N_fR products at m/z 69–75 and about 101, which cannot originate from 1,4-dioxane.

$[M + H]^+$ of 1-Aza-18-Crown-6 (6). Substitution of one O by NH in polyether **5** dramatically changes the unimolecular chemistry of the corresponding $[M + H]^+$ cation. This is evident from comparison of the CAD spectra of $[6 + H]^+$ (Figure 6) and $[5 + H]^+$ (Figure 4b). The aza precursor yields many more fragments, all of which can be envisioned to result from charge-remote fragmentations from ring-opened isomers (Schemes IV and V and following discussion).

Owing to the larger proton affinity of amines versus that of ethers [30], protonation of **6** should take place at the NH functionality and form an ammonium cation. Such ions possess a well stabilized charge center and have been found to favor charge-remote fragmentations upon CAD [10, 31]. A viable route to the CAD products of $[6 + H]^+$ begins with homolytic ring-opening accompanied by hydrogen atom migrations to yield the immonium cations $\mathbf{6a}^+$ and $\mathbf{6b}^+$ (Scheme IV); these ions are produced by initial cleavages of a

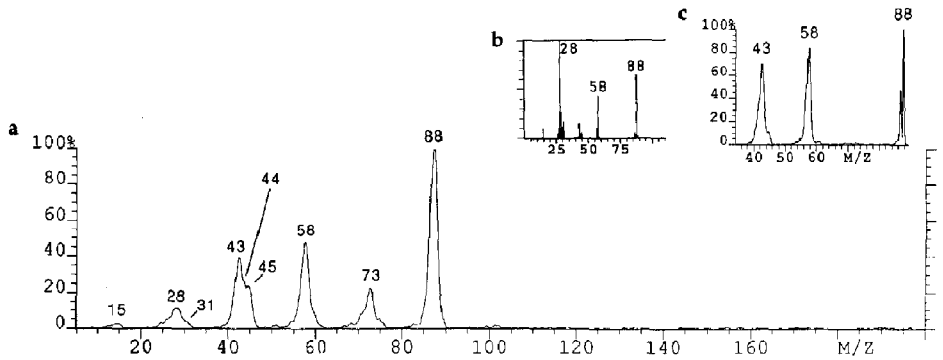

Figure 5. (a) N_fR mass spectrum of protonated 18-crown-6, $[5 + H]^+$ (m/z 265) (b) Electron ionization [26] and (c) partial neutralization-reionization mass spectra of 1,4-dioxane.

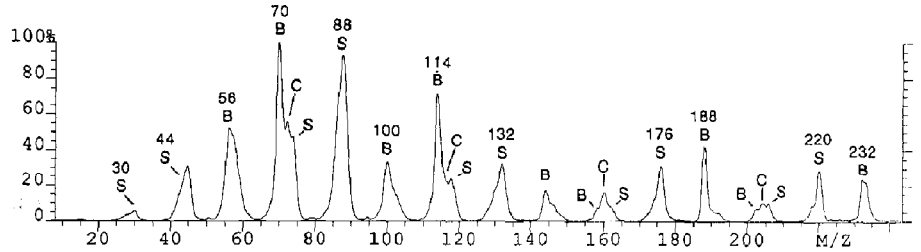

Figure 6. CAD mass spectrum of protonated 1-aza-18-crown-6, $[6 + H]^+$ (m/z 264). The **B**, **C**, and **S** series marked appear at the m/z values given in Scheme V.

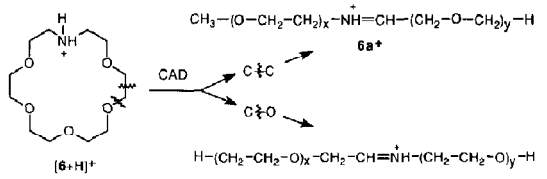

Scheme IV

C—C or C—O bond, respectively. Charge-remote decompositions of $\mathbf{6a}^+$ and $\mathbf{6b}^+$ can account for all major CAD fragment ions from $[\mathbf{6} + H]^+$. These ions have been classified in Scheme V according to their termini, with the **B** series containing a vinyl, the **C** series a formyl, and the **S** series a saturated end group.

Charge-site-initiated reactions of $[\mathbf{6} + H]^+$, analogous to those observed for $[\mathbf{5} + H]^+$, would involve losses of $(C_4H_8O_2)_n$ (see Scheme III) and lead to an **A** series at m/z 44, 88, 132, 176, and 220. This series is isobaric with the **S** series, which arises by charge-remote fragmentations from $\mathbf{6a}^+$ (see Scheme V). The **A** and **S** series liberate different neutral losses and should be distinguishable from N_fR spectra. A substantial amount of **A** type fragments from $[\mathbf{6} + H]^+$ should coproduce a measurable amount of 1,4-dioxane molecules that, as previously discussed, contribute several diagnostic peaks to the N_fR spectrum, for example, at m/z 88 (see Figure 5). However, the N_fR spectrum of $[\mathbf{6} + H]^+$ (Figure 7) does not show a distinct m/z 88 signal and is markedly different from the N_fR spectrum of $[\mathbf{5} + H]^+$ (Figure 5), which does eliminate 1,4-dioxane (vide supra). Normalized to the flux of all neutral losses, the abundance of m/z 88 in Figure 7 is $< 6\%$ of [m/z 88] in Figure 5. Evidently, charge-initiated dissociations, which would generate dioxane, are not preferred by the aza ion $[\mathbf{6} + H]^+$.

The neutral fragment mixture from the charge-

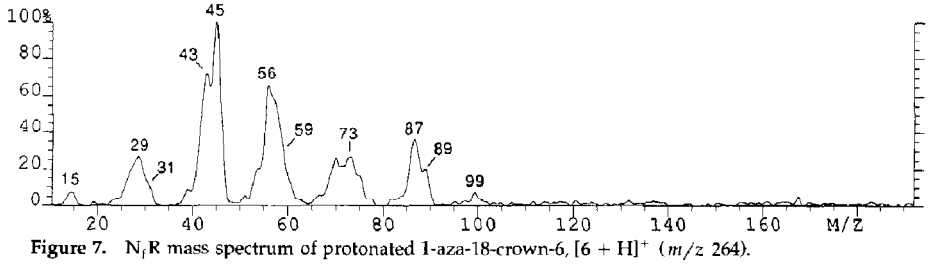

Figure 7. N_fR mass spectrum of protonated 1-aza-18-crown-6, $[\mathbf{6} + H]^+$ (m/z 264).

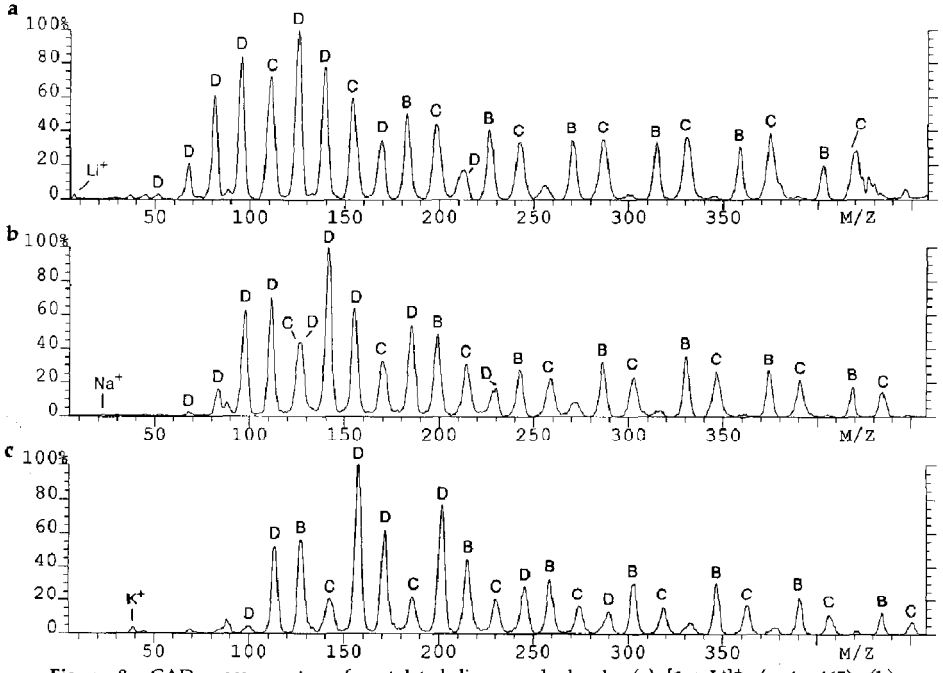

Figure 8. CAD mass spectra of metalated linear polyglycols: **(a)** $[\mathbf{1} + Li]^+$ (m/z 465), **(b)** $[\mathbf{1} + Na]^+$ (m/z 481), and **(c)** $[\mathbf{1} + K]^+$ (m/z 497). The **B**, **C**, and **D** series marked appear at the mass-to-charge ratio values given in Schemes VI and VII.

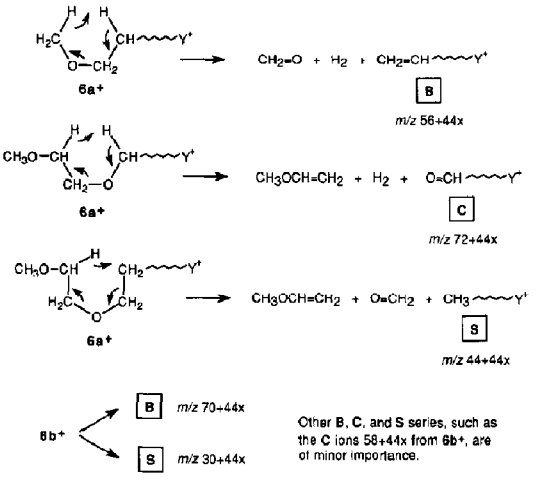

Scheme V

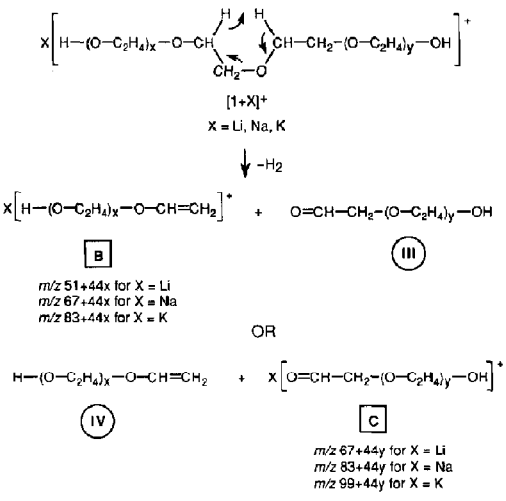

Scheme VI

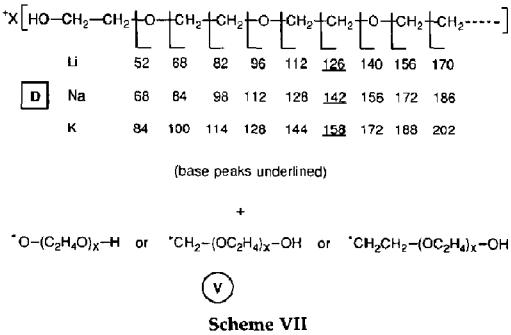

Scheme VII

remote fragmentations of $[6 + H]^+$ is mainly composed of

$$H{-}(CH_2OCH_2)_n{-}CH{=}O,$$
$$H{-}(CH_2OCH_2)_n{-}CH_2OCH{=}CH_2,$$
$$O{=}CH{-}(CH_2OCH_2)_n{-}CH_2OH,$$

and

$$H{-}(CH_2CH_2O)_n{-}CH{=}CH_2$$

(see Scheme V). These neutrals give rise to a unique N_fR spectrum (Figure 7). Complete interpretation of this spectrum is not possible because of the absence of suitable reference CIDI mass spectra; nonetheless, Figure 7 provides useful mechanistic insight by being distinct from the N_fR spectrum of $[5 + H]^+$ and, thus, precluding that $C_4H_8O_2$ losses from the aza precursor $[6 + H]^+$ occur to any significant degree.

$[M + X]^+$ Precursor Ions with X = Li, Na, and K

$[M + X]^+$ from Poly(ethylene glycol) Decamer (1). The unimolecular reactions of collisionally activated $[1 + X]^+$ lead to fairly similar CAD spectra irrespective of the cationizing metal (Figure 8). The dominant fragment ions belong to three series, which can be rationalized by two different types of charge-remote fragmentations [6]. **B** and **C** ions arise by charge-remote 1,4-H_2 eliminations, as shown in Scheme VI. Such reactions produce two terminally unsaturated species, either of which may keep the metal ion. Following the classification introduced previously, the **B** series terminates with a $H_2C{=}CH$ and the **C** series with a $O{=}CH$ functionality. An additional group of fragments corresponds to nominal losses of radicals that yield the **D** type distonic radical cations described in Scheme VII. The complete **B** and **C** series are obtained for all three metal attachment cations studied (Figure 8; some low mass members of **B** or **C** are not well resolved from adjacent stronger **D** ions). In contrast, only the low mass **D** ions appear with measurable abundances. The formation of small radical cations from metalated closed-shell precursors is not unique to polyglycols. Such behavior has been encountered previously with lithiated fatty acids and alcohols [32, 33].

The following spectral features are worth noting:

1. The relative intensities of **B** and **C** fragments are quite similar, in keeping with the mechanism of Scheme VI. The fraction of **C** ions, in which both termini contain O atoms, slightly increases as the size of the metal ion decreases, which suggests a rising affinity for oxygen in the order $Li^+ > Na^+ > K^+$.
2. All three $[1 + X]^+$ precursors yield the same **D** ion, $^+X[HO{-}(CH_2CH_2O)_2{-}CH_2^{\cdot}$, as base peak (Scheme VII).
3. The most prominent **B** and **C** ions from all three $[1 + X]^+$ contain 2–4 monomer units. Such analogies suggest that Li^+, Na^+, and K^+ attach to a common site. Because low mass fragment ions are preferentially formed (see Figure 8), the metal ion

probably adds at or near the terminal PEG positions.

The **B**, **C**, and **D** sequence ions also are observed in low energy CAD spectra, although with smaller relative intensities [6]. These spectra are dominated by an **A** series, proposed to emerge via charge-induced cleavages as shown in Scheme VIII [6]. **A** type ions are basically absent under kiloelectronvolt collision conditions (Figure 8), where more internal energy is available. The discrimination against **A** fragments in high energy CAD points out that X^+ catalyzed reactions have lower critical energies but more severe entropic constraints than charge-remote pathways. As a consequence, **A** products are favored over **B**, **C**, and **D** fragments in low energy CAD and vice versa.

Under low energy CAD conditions, $[1 + Na]^+$ was found to mainly yield Na^+ and very little sodiated product ions of type **A**, **B**, **C**, or **D** [6]. At the energy levels attainable in the present experiments, the latter organic ions are formed with comparable efficiencies from all three $[1 + X]^+$. Dissociation to X^+ also takes place, but its yield is miniscule judging from the relative abundances of Li^+, Na^+, and K^+ in the CAD spectra of Figure 8; the very low abundance of X^+ may be due to the substantial scattering of these small ions [29].

The N_fR spectra of $[1 + Li]^+$, $[1 + Na]^+$, and $[1 + K]^+$ (not shown) are quite similar, which verifies that comparable neutral mixtures are liberated from these three precursor ions. They also resemble the N_fR spectrum of ion $[1 + H]^+$ (Figure 2a), which was shown to cleave PEGs upon CAD (type **I** neutrals in Scheme I). According to Schemes VI and VII, the major neutral losses from $[1 + X]^+$ are molecules of type **III** and **IV** and radicals of type **V**. All of these species include a glycol terminus. It is not surprising therefore that, on post-ionization, they form fragments common to those from reionization of type **I** neutrals. Compared to

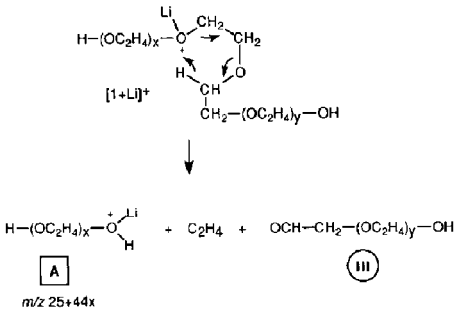

Scheme VIII

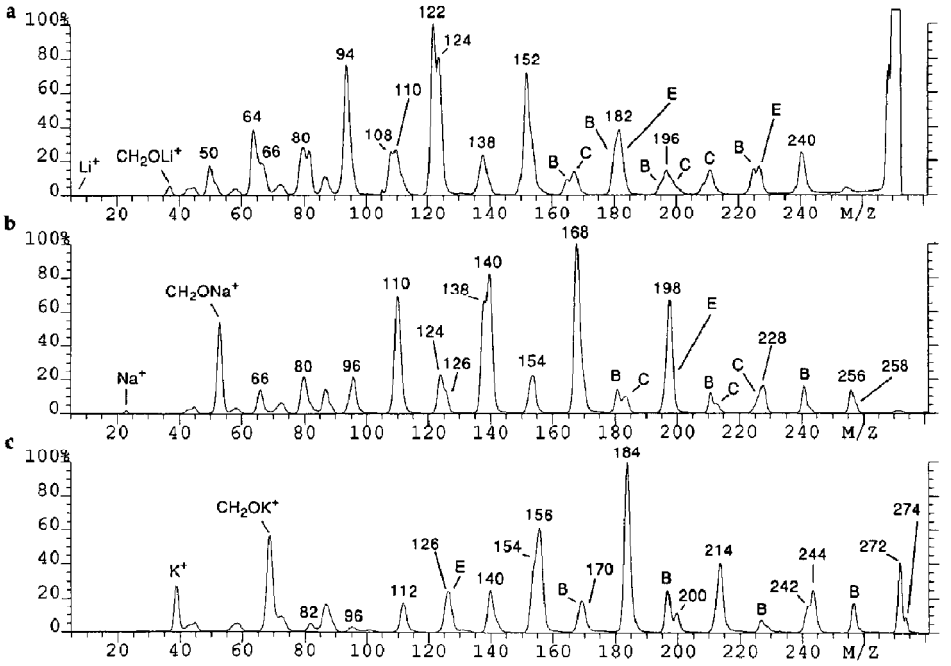

Figure 9. CAD mass spectra of metalated 18-crown-6: **(a)** $[5 + Li]^+$ (m/z 271), **(b)** $[5 + Na]^+$ (m/z 287), and **(c)** $[5 + K]^+$ (m/z 303). The peaks that belong to the **D** series are marked by their mass-to-charge ratio values; **D** ions of the same composition can arise from $\mathbf{5a}^+$ or $\mathbf{5b}^+$ (Scheme IX). Type **B**/**C** ions that can be formed from intermediate $\mathbf{5a}^+$ are observed at **(a)** m/z 167, 181, 195, 211, and 225; **(b)** m/z 183, 211, 227, and 241; **(c)** m/z 169, 227, and 257. **B**/**C** ions that can be formed from intermediate $\mathbf{5b}^+$ are observed at **(a)** m/z 165, 181, 197, and 225; **(b)** m/z 181, 213, and 241; **(c)** m/z 169, 197, and 257. For the mass-to-charge ratio values of the **E** series, see text.

Figure 2a, the N_fR spectra of $[1 + X]^+$ contain more unsaturated products, for example, at m/z 43, 69–73, and 87 (base peak). Presumably, these extra ions originate from the formyl end of **III**, the vinyl end of **IV**, and/or the radical bearing end of **V**.

$[M + X]^+$ from 18-Crown-6 (5). CAD of $[5 + X]^+$ primarily yields **D** type radical cations by elimination of $C_nH_{2n+1}O_m^{\cdot}$ radicals (Figure 9; all peaks with marked mass-to-charge ratio values belong to series **D**). For example, the two most prominent fragment ions from $[5 + Li]^+$ (m/z 122 and 124) arise by losses of $C_6H_{13}O_4^{\cdot}$ (149 u) and $C_7H_{15}O_3^{\cdot}$ (147 u), and the base peaks of both $[5 + Na]^+$ (m/z 168) and $[5 + K]^+$ (m/z 184) stem from loss of $C_5H_{11}O_3^{\cdot}$ (119 u). Such products are most likely formed by charge-remote fragmentations from open-chain isomers (vide infra).

The measured K^+ affinity of **5** is 167 kJ/mol [34]; **5**'s Li^+ and Na^+ affinities have not been determined, but should be comparably high based on the fairly similar Li^+, Na^+, and K^+ selectivities of this crown ether [35]. Consequently, X^+ is strongly bonded in the $[5 + X]^+$ adduct and should show no tendency for initiating charge-site decompositions on CAD. Instead, scission of charge-remote C—C or C—O bonds could take place and lead, after concomitant hydrogen atom transfers, to the ring-opened isomers $\mathbf{5a}^+$ or $\mathbf{5b}^+$, respectively (Scheme IX). Homolytic bond cleavages in these intermediates by a mechanism parallel to that of Scheme VII generate the observed **D** series. For example, cleavage of $CH_3—(OC_2H_4)_2—O^{\cdot}$ (119 u) from $\mathbf{5a}^+$ produces the base peak for X = Na (m/z 168) and

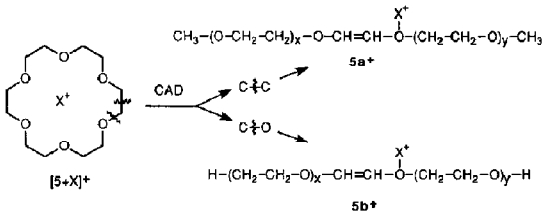

Scheme IX

K (m/z 184), whereas cleavage of $^{\cdot}O—(C_2H_4O)_3—H$ (149 u) from $\mathbf{5b}^+$ gives rise to the base peak for X = Li (m/z 122). Similarly, loss of $CH_3—(OC_2H_4)_3^{\cdot}$ from $\mathbf{5a}^+$ or of $H—(C_2H_4O)_3—CH_2^{\cdot}$ from $\mathbf{5b}^+$ (the mass of both radicals is 147 u) forms the second most abundant ion for X = Li (m/z 124), etc. The rupture of larger radicals generally becomes less pronounced as the size of the metal ion increases.

It is noticed that only saturated radicals ($C_nH_{2n+1}O_m^{\cdot}$) are eliminated from $[5 + X]^+$. The absence of any significant $C_nH_{2n-1}O_m^{\cdot}$ losses indicates that the unsaturation (double bond) created upon ring-opening ends up very close to the X^+ charge center, as in $\mathbf{5a}^+$ and $\mathbf{5b}^+$. The open-chain isomers $\mathbf{5a}^+$ and $\mathbf{5b}^+$ can also undergo charge-remote 1,4-H_2 eliminations by pathways similar to those shown in Schemes V and VI for related precursor ions. Such reactions account for the **B** and **C** fragments observed in Figure 9. Another interesting feature of Figure 9 is the decreasing abundance of X^+ from $K^+ \rightarrow Na^+ \rightarrow Li^+$; apparently, the ease of demetalation, that is, of breaking

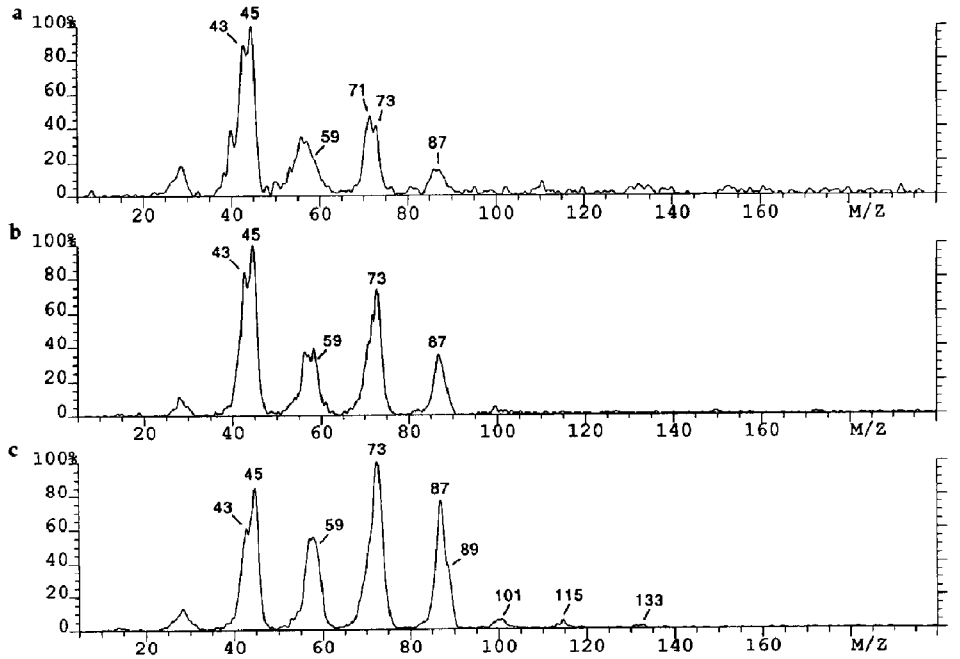

Figure 10. N_fR mass spectra of metalated 18-crown-6: (**a**) $[5 + Li]^+$ (m/z 271), (**b**) $[5 + Na]^+$ (m/z 287), and (**c**) $[5 + K]^+$ (m/z 303).

the $5 - X^+$ bond, ascends with the size of the metal ion.

The losses of $(C_2H_4O)_n$, which dominated the CAD spectrum of protonated **5**, are miniscule for the metalated crown ether. The only discernible products that corresponds to such eliminations (termed type **E**) are $[5 + Li - C_2H_4O]^+$ (m/z 227), $[5 + Li - C_4H_8O_2]^+$ (m/z 183), $[5 + Na - C_4H_8O_2]^+$ (m/z 199), and $[5 + K - C_8H_{16}O_4]^+$ (m/z 127); the three latter products appear as shoulders of adjacent **D** ions of one mass unit lower. The $(C_2H_4O)_n$ cleavages from $[5 + H]^+$ could proceed by a mechanism analogous to that of Scheme III and lead to cyclic **E** ions. The very low abundance of series **E** in Figure 9 suggests that such a process, that is, fragmentation without ring opening (be it charge catalyzed or charge remote), cannot compete effectively with dissociations via the open-chain forms $\mathbf{5a}^+$ or $\mathbf{5b}^+$.

A common characteristic of all three $[5 + X]^+$ cations is the preference for charge-remote reactions that produce distonic radical ions of class **D**; **D** ions also are favored upon low energy CAD conditions [9]. The complementary neutral fragments are radicals with the general formula $C_nH_{2n+1}O_m^{\cdot}$ and $n - 6 \leq m \leq n$, depending on which bond in $\mathbf{5a}^+$ or $\mathbf{5b}^+$ (Scheme IX) is broken. These species and all other (minor) neutral losses from $[5 + X]^+$ yield, after reionization, the N_fR spectra of Figure 10. Similar peak groups are observed in the individual N_fR spectra, but their absolute abundances (reflected in the signal to noise ratio) and relative amounts vary. These variations may reflect the generation of different proportions of $\mathbf{5a}^+$ and $\mathbf{5b}^+$ from the three different $[5 + X]^+$ ions.

Conclusions

The unimolecular chemistry of cationized polyglycols with high energy CAD is strongly dependent on both the nature of the charge site and the structure of the polyglycol. Protonated precursors that contain solely ether (and alcohol) functionalities mainly undergo charge-induced dissociations. In sharp contrast, metalated precursors or protonated precursors with amine substituent(s) predominantly fragment by charge-remote reactions. Evidently, metal ion attachment or amine protonation lead to tightly bound well stabilized charge centers with the result that breakup of charge-remote bonds costs less energy.

An interesting finding of this study is the generation of a large amount of distonic radical ions from the metalated precursors (especially from the cyclic molecule). The preferential generation of such open-shell products from closed-shell $[M + X]^+$ may be due to a high thermodynamic stability for metalated distonic ions, possibly incurred by interactions between the alkali cation and the unpaired electron.

Overall, high energy CAD is found to produce fragment ions over the entire mass range. Precursor ions that undergo charge-remote decompositions yield several types of abundant and structure diagnostic fragment series and are, thus, uniquely suitable for the determination of unknown polyglycol sequences.

Acknowledgment

The National Institutes of Health and the Ohio Board of Regents are thanked for generous financial support. We are grateful to Michael J. Polce, Blas Cerda, Šárka Beranová, and Marcela M. Cordero for experimental assistance and discussions.

References

1. Busch, K. L.; Glish, G. L.; McLuckey, S. A. *Mass Spectrometry/Mass Spectrometry*, VCH Publishers: New York, 1988.
2. Harrison, A. G.; Cotter, R. J. *Methods Enzymol.* **1990,** *193,* 3–36.
3. Lyon, P. A.; Stebbings, W. L.; Crow, F. W.; Tomer, K. B.; Lippstreu, D. L.; Gross, M. L. *Anal. Chem.* **1984,** *56,* 8–13.
4. Lyon, P. A.; Crow, F. W.; Tomer, K. B.; Gross, M. L. *Anal. Chem.* **1984,** *56,* 2278–2284.
5. Lattimer, R. P.; Munster, H.; Budzikiewicz, H. *Int. J. Mass Spectrom. Ion Processes* **1989,** *90,* 119–129.
6. Lattimer, R. P. *J. Am. Soc. Mass Spectrom.* **1992,** *3,* 225–234.
7. Liou, C.-C.; Brodbelt, J. S. *J. Am. Soc. Mass Spectrom.* **1992,** *3,* 543–548.
8. Lattimer, R. P. *Int. J. Mass Spectrom. Ion Processes* **1992,** *116,* 23–36.
9. Lattimer, R. P. *J. Am. Soc. Mass Spectrom.* **1994,** *5,* 1072–1080.
10. Adams, J. *Mass Spectrom. Rev.* **1990,** *9,* 146–181.
11. Wesdemiotis, C.; McLafferty, F. W. *Chem. Rev.* **1987,** *87,* 485–500.
12. Terlouw, J. K.; Schwarz, H. *Angew. Chem. Int. Ed. Engl.* **1987,** *26,* 805–815.
13. Holmes, J. L. *Mass Spectrom. Rev.* **1989,** *8,* 513–539.
14. Cordero, M. M.; Wesdemiotis, C. In *Biological Mass Spectrometry: Present and Future*; Matsuo, T.; Caprioli, R. M.; Gross, M. L.; Seyama, Y., Eds.; Wiley: New York, 1994; p 119.
15. Burgers, P. C.; Holmes, J. L.; Mommers, A. A.; Terlouw, J. K. *Chem. Phys. Lett.* **1983,** *102,* 1–3.
16. Holmes, J. L.; Hop, C. E. C. A.; Terlouw, J. K. *Org. Mass Spectrom.* **1986,** *21,* 776–778.
17. Cordero, M. M.; Houser, J. J.; Wesdemiotis, C. *Anal. Chem.* **1993,** *65,* 1594–1601.
18. Cordero, M. M.; Wesdemiotis, C. *Org. Mass Spectrom.* **1993,** *28,* 1041–1046.
19. Cordero, M. M.; Wesdemiotis, C. *Anal. Chem.* **1994,** *66,* 861–866.
20. Polce, M. J.; Cordero, M. M.; Wesdemiotis, C.; Bott, P. A. *Int. J. Mass Spectrom. Ion Processes* **1992,** *113,* 35–58.
21. Wesdemiotis, C.; Leyh, B.; Fura, A.; McLafferty, F. W. *J. Am. Chem. Soc.* **1990,** *112,* 8655–8660.
22. Levsen, K. *Fundamental Aspects of Organic Mass Spectrometry*; Verlag Chemie: Weinheim, Germany, 1978.
23. Lias, S. G.; Bartmess, J. E.; Liebman, J. F.; Holmes, J. L.; Levin, R. D.; Mallard, W. G. *J. Phys. Chem. Ref. Data* **1988,** *17,* Suppl. 1.
24. Vekey, K.; Brenton, A. G. *Rapid Commun. Mass Spectrom.* **1988,** *2,* 156–161.
25. Beranová, Š.; Wesdemiotis, C. *J. Am. Soc. Mass Spectrom.* **1994,** *5,* 1093–1101.
26. McLafferty, F. W.; Stauffer, D. B. *Wiley/NBS Registry of Mass Spectral Data*; Wiley: New York, 1988.
27. Lee, Y. C.; Popov, A. I.; Allison, J. *Int. J. Mass Spectrom. Ion Phys.* **1983,** *51,* 267–277.

28. Huang, S. K.; Allison, J. *Organometallics* **1983,** *2,* 883–890.
29. Li, X.; Harrison, A. G. *J. Am. Chem. Soc.* **1993,** *115,* 6327–6332.
30. Lias, S. G.; Liebman, J. F.; Levin, R. D. *J. Phys. Chem. Ref. Data* **1984,** *13,* 695–808.
31. Wysocki, V. H.; Ross, M. M.; Horning, S. R.; Cooks, R. G. *Rapid Commun. Mass Spectrom.* **1988,** *2,* 214–216.
32. Adams, J.; Gross, M. L. *Anal. Chem.* **1987,** *59,* 1576–1582.
33. Adams, J.; Gross, M. L. *J. Am. Chem. Soc.* **1986,** *108,* 6915–6921.
34. Katritzky, A. R.; Malhotra, N.; Ramanathan, R.; Kemerait, R. C., Jr.; Zimmerman, J. A.; Eyler, J. R. *Rapid Commun. Mass Spectrom.* **1992,** *6,* 25–27.
35. Maleknia, S.; Brodbelt, J. *J. Am. Chem. Soc.* **1992,** *114,* 4295–4298.